Author's personal copy

Palaeogeography, Palaeoclimatology, Palaeoecology 306 (2011) 1–14

Contents lists available at ScienceDirect

Palaeogeography, Palaeoclimatology, Palaeoecology

journal homepage: www.elsevier.com/locate/palaeo

Molecular and petrographic indicators of redox conditions and bacterial communities after the F/F mass extinction (Kowala, Holy Cross Mountains, Poland)

Leszek Marynowski [a,*], Michał Rakociński [a], Ewelina Borcuch [a], Barbara Kremer [b], Brian A. Schubert [c], A. Hope Jahren [c]

[a] University of Silesia, Faculty of Earth Sciences, Będzińska Str. 60, 41-200 Sosnowiec, Poland
[b] Institute of Paleobiology, Polish Academy of Sciences, Twarda 51/55, 00-818 Warszawa, Poland
[c] Department of Geology and Geophysics, University of Hawaii, Honolulu, Hawaii, 96822, USA

ARTICLE INFO

Article history:
Received 27 November 2010
Received in revised form 22 February 2011
Accepted 18 March 2011
Available online 24 March 2011

Keywords:
Pyrite framboids
Cyanobacteria
Biomarkers
Redox conditions
Organic geochemistry
Mass extinction

ABSTRACT

Pyrite framboid diameter analysis and organic geochemistry of the *triangularis*/*crepida* boundary section at Kowala (Holy Cross Mountains, Poland) imply suboxic to oxic and sporadically euxinic bottom waters during the Lower Famennian. In addition, morphological web-like structures typical for microbial mats, as well as the recognition of 2α-methylhopanes and monomethyl-alkane cyanobacteria biomarkers is evidenced of microbial activity after the global Frasnian/Famennian (F/F) extinction event. The presence of cyanobacterial mats also suggests suboxic to oxic environments and at the same time photic bottom water conditions. However, isorenieratane and its derivatives were detected in almost all samples. The presence of this well-known biomarker of green sulfur bacteria implies that euxinic conditions were present in the upper part of the water column at least intermittently or that temporal euxinia occurred in the water column. Presence of euxinic conditions is confirmed by the occurrence of small-sized pyrite framboids which were particularly dominant in the lower part of the section. The shift towards low $\delta^{13}C$ values in both micritic limestones and in sedimentary organic matter seen at the beginning of the period of diminished photic zone, might reflect an influx of newly respired CO_2 to surface waters, caused by enhanced respiration at depth after the F/F transition in the Chęciny–Zbrza basin.

© 2011 Elsevier B.V. All rights reserved.

1. Introduction

Reduced animal diversity after mass extinction events gives rise to enhanced productivity of microbial communities (e.g. Sheehan and Harris, 2004; Xie et al., 2005) because mat-inhibiting animals have been removed from ecosystems and marine productivity is generally low. One example is the microbial expansion observed after the Permo/Triassic (P/Tr) mass extinction; this increase in microbial activity is inferred from post-extinction sedimentary rocks (Schubert and Bottjer, 1992; Kershaw et al., 1999; Lehrmann et al., 2003; Pruss and Bottjer, 2004; Baud et al., 2005, 2007; Kershaw et al., 2007; Mary and Woods, 2008; Woods and Baud, 2008). Detailed studies using cyanobacterial biomarkers across the P/Tr boundary revealed variations in the microbial community structure with cyanobacteria expansion after the P/Tr mass extinction event (Xie et al., 2005, 2007; Wang, 2007), recently associated with volcanic activity (Xie et al., 2010). Surprisingly, much less is known about microbial activity after other mass extinction events. Reports on the Late Ordovician extinction event revealed microbialite resurgence (Sheehan and Harris, 2004). Similar work showed expansion of opportunistic stromatolites, oncoids, and large-scale microbial thrombolites after the Frasnian–Famennian (F/F) mass extinction (Becker et al., 1991; Whalen et al., 2002; see also Racki et al., 2002). Finally, elevated concentrations of cyanobacteria biomarkers have been reported across the Triassic/Jurassic extinction boundary (Jiao et al., 2009).

Kowala, Poland is one of the best documented high-resolution sections that includes the F/F transition (see e.g. Racki et al., 2002) and has been investigated using paleontological (Racki and Baliński, 1998; Sartenaer et al., 1998; Dzik, 2002; Filipiak, 2002; Ginter, 2002; Vishnevskaya et al., 2002; Bond, 2006), petrographic (Bond et al., 2004), organic and inorganic geochemical (Joachimski et al., 2001; Girard and Lécuyer, 2002; Racki et al., 2002; Bond and Zatoń, 2003; Bond et al., 2004) and isotopic (Joachimski et al., 2001, 2002) techniques. Although the F/F stratigraphic boundary in Kowala is well studied, little has been written about microbial communities in the Early Famennian, particularly regarding any hypothetical increase in microbial activity after the F/F biotic crisis.

Here we report the presence of cyanobacteria biomarkers in the Early Famennian portion of the Kowala section, as confirmed by scanning electron microscope observations of fossil cyanobacterial colonies. In addition, we detail the biogeochemical characteristics of redox conditions using a combination of organic-biomarker and

* Corresponding author.
E-mail address: leszek.marynowski@us.edu.pl (L. Marynowski).

0031-0182/$ – see front matter © 2011 Elsevier B.V. All rights reserved.
doi:10.1016/j.palaeo.2011.03.018

Author's personal copy

pyrite petrographic data. The data confirmed the common expansion of cyanobacterial communities after global mass extinctions also in the basinal environments with low light intensity and described detailed characteristic of the post-extinction water column structure.

2. Geological background and previous geochemical studies

The Kowala quarry is located in the southern limb of the Gałęzie-Kowala syncline, within the southern part of the Kielce region of the Holy Cross Mountains (HCM), approximately 10 km SW of Kielce, Poland (Fig. 1a and b) (see e.g., Racki et al., 2002). Many papers have characterized the Famennian section in the Kowala quarry, including Racki and Szulczewski (1996), Berkowski (2002), Racki et al. (2002), Bond and Zatoń (2003), Dzik (2006), Marynowski and Filipiak (2007), Marynowski et al. (2007, 2010) and Halamski and Baliński (2009). During the Late Devonian the Holy Cross Mountains were part of a ≤600 km wide carbonate shelf. This region comprised a portion of the pericratonic basin extending along the southern margin of Laurussia (e.g. Narkiewicz, 1988; Racki and Baliński, 1998; Joachimski et al., 2001; Racki et al., 2002). The Devonian paleogeography of the HCM is characterized by two major distinct tectonic regions: the Kielce paleohigh in the south and the Łysogóry paleolow to the north. These subsymmetric facies occur in the center of the Frasnian Dyminy reef and the Famennian remnant pelagic ridge (see Szulczewski, 1971, 1995; Racki and Baliński, 1998; Racki et al., 2002). These features were surrounded by two intrashelf basins: the Chęciny–Zbrza to the south and the Łysogóry–Kostomłoty to the north. The study area is located within in the Chęciny–Zbrza intra-shelf basin. Lower Famennian successions are represented by a monotonous series of thin- and rhythmically-bedded marly limestones and shales which are poor in fossils (Racki and Szulczewski, 1996). The depositional environment is interpreted as poorly oxygenated and open-marine, and deep-water below storm wave-base; there is also an expanded base of slope to basinal succession (see e.g. Racki et al., 2002; Bond and Zatoń, 2003; Bond et al., 2004; Filipiak, 2009).

The Famennian sequence has been divided into informal lithological sets H to L (in Racki and Szulczewski, 1996; see also Berkowski, 2002); however, here we describe only the lithology of the currently analyzed part of the section (Fig. 1c). Our investigated sections belong to the set H-4 (*sensu* Racki and Szulczewski, 1996) and were assigned to the Upper *Palmatolepis triangularis* zone and the lower part of the *Palmatolepis crepida* zone (see Section 4.1). This dating corresponds to palynostratigraphic data provided by Filipiak (2009), which particularly distinguished the Pw acritarch zone. The upper part of the section is notable for its rare *Guerichia* and inarticulate brachiopods including the lingulid *Barroisella* and *Orbiculoidea* (see also Berkowski, 2002; Racki et al., 2002; Bond and Zatoń, 2003), and rare undeterminable orthoconic nautiloids. In addition, Filipiak (2009) described rich and well-preserved phytoplankton assemblages containing mainly acritarchs and prasinophytes, as well as a low-diversity miospore microflora.

Until now geochemical studies of the Frasnian and Famennian portions of the Kowala section have concentrated on describing potentially global phenomena (Fig. 2), during either the F/F transition climate change (Joachimski et al., 2001, 2002; Girard and Lécuyer, 2002; Racki et al., 2002; Bond and Zatoń, 2003; Bond et al., 2004), or the Hangenberg event (Marynowski and Filipiak, 2007), or the Dasberg event (Marynowski et al., 2010). Other works focused upon specific subsections of the Kowala section, such as the Middle Famennian interval with its pyritized fauna (Marynowski et al., 2007) or the Early–Middle Frasnian transition (Marynowski et al., 2008). Here we present multi-proxy studies of the sequences belonging to the Upper *P. triangularis* zone and the lower part of the *P. crepida* zone as the first such studies of this critical portion of the post-F/F transition into the Early Famennian (Fig. 2).

3. Materials and methods

Fifteen samples were collected from the trench of the central part of the active Kowala Quarry (Fig. 1a and b). The investigated strata consisted of rhythmic successions of dark gray micritic limestones and dark gray or black marly shales; the thickness of the section investigated was approximately 4 m. Micritic limestones and marly shales were sampled and studied for geochemistry and petrography. Nine samples were studied for conodont biostratigraphy.

3.1. Micropaleontological preparation

Nine samples were used to obtain conodont elements. The samples of 800–1000 g weight were dissolved in 15% formic acid or in 20% acetic acid. The resultant sediment was rinsed using a sieve with 0.1 mm diameter meshes. Conodonts in marl samples were separated via sodium polytungstate solution with 2.78–2.84 g/ml specific weight. Isolated conodont samples were examined using binocular microscopy.

3.2. Cyanobacterial mat microscopic observations

All petrographic thin sections were polished to 0.25 μm using diamond paste, etched with 5% and 8% formic acid, rinsed in DI water, dried, and gold-coated to facilitate conductivity. Prior to scanning electron microscopy, all petrographic thin sections were scrutinized and mapped by conventional optical microscopy. The SEM investigations used either a Zeiss DSM 960A equipped with an EDS detector (Bruker-AXS) at Ludwig Maximillian University (Munich, Germany) and a JEOL JEM-3010 equipped with a Gatan slow scan CCD camera at Philipps University (Marburg, Germany).

3.3. Pyrite framboid diameter analysis

Thirteen samples were used for the pyrite framboid analysis. Samples in the form of small chips were polished, and framboid diameters were measured using the Philips Environmental Scanning Electron Microscope in a back-scattered electron mode at University of Silesia (Sosnowiec, Poland). Framboid diameters were measured using the ESEM internal measuring device (given in μm). In seven of the ten samples, at least 100 framboids were measured; in three samples this was not possible. For each sample, such statistical parameters (see Wignall and Newton, 1998) as minimum and maximum values, mean value and standard deviation have been calculated, and then shown in the form of box-and-whisker plots.

3.4. Isotope analysis

Stable isotope determinations were performed upon samples KclII/1, 3, 4, 7, 9, 10, 11, 13, 16, 17 and 19 (Fig. 1c). Organic carbon was extracted from rock samples by digestion in 1 M HCl for 24 h at 25 °C. The remaining organic fraction was homogenized and combusted in triplicate using a Eurovector EA in conjunction with an Isoprime IRMS to obtain $\delta^{13}C$ values (Boutton, 1991). The $\delta^{13}C$ and $\delta^{18}O$ values of carbonate were obtained through classical methods, which involve reaction of sample carbonate with phosphoric acid and the purification of resultant CO_2 gas for measurement on dual inlet (McCrea, 1950). All measurements were performed using the IRMS facility of the University of Hawaii, and are reported using standard "delta-notation" relative to VSMOW and VPBD standards (Sharp, 2006).

3.5. Organic geochemistry

Abundances of total carbon and total inorganic carbon were determined using an Eltra CS-500 IR-analyzer with a total inorganic carbon module. Total organic carbon (TOC) was calculated as the difference between total carbon and total inorganic carbon. Calibration

Author's personal copy

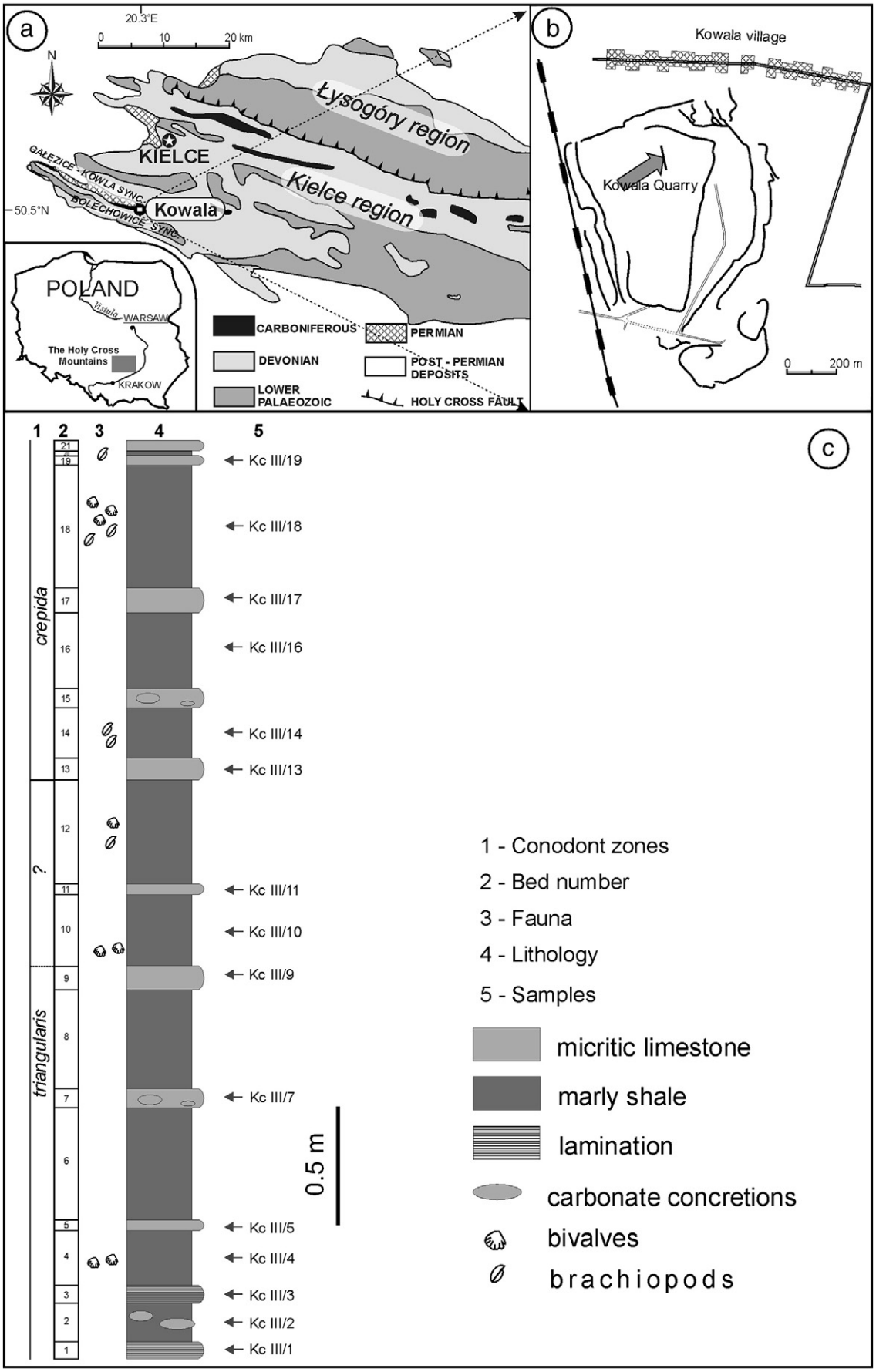

Fig. 1. Schematic geological map of the western and central parts of the Holy Cross Mountains (a) with location of the Kowala Quarry (b) and investigated section (c). Map is adopted from Marynowski et al. (2007) paper.

Author's personal copy

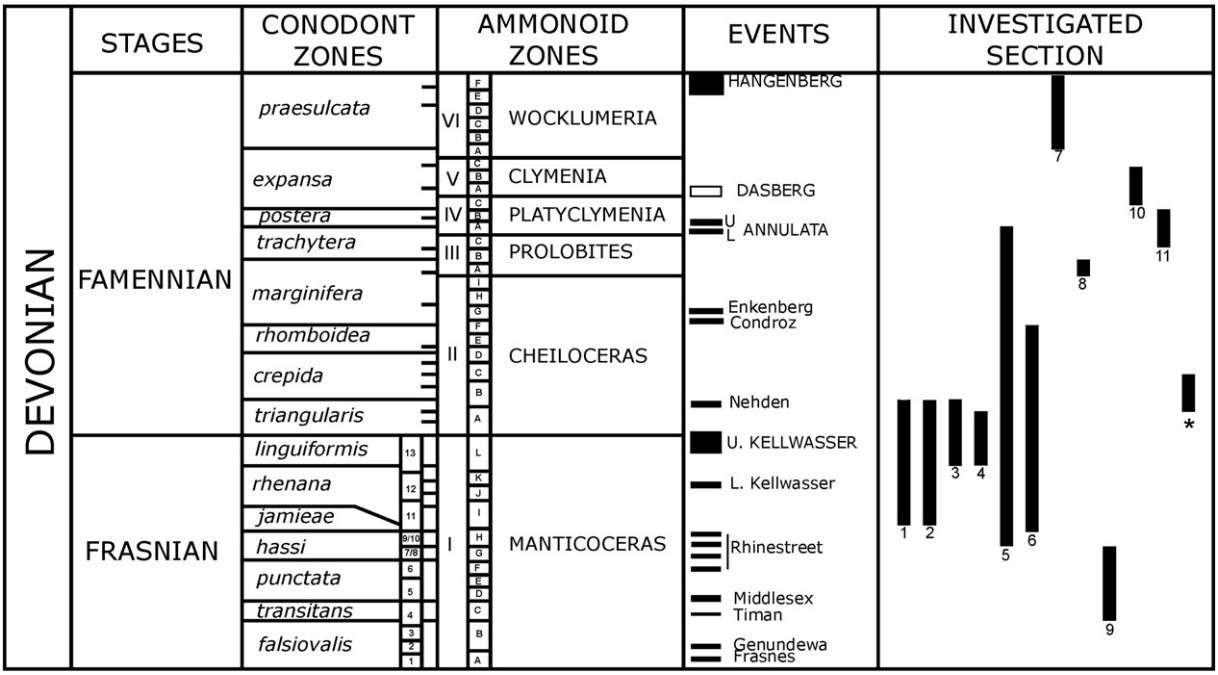

Fig. 2. Diagram showing the correspondence of the main 'events' recognized in the Late Devonian with the chronostratigraphic stages and with conodont and ammonoid zonations (based on House, 2002, slightly modified); including previously investigated parts of the Kowala section by geochemical and petrographical methods : 1 — Joachimski et al. (2001); 2 — Joachimski et al. (2002); 3 — Racki et al. (2002); 4 — Girard and Lécuyer (2002); 5 — Bond and Zatoń (2003); 6 — Bond et al. (2004); 7 — Marynowski and Filipiak (2007); 8 — Marynowski et al. (2007); 9 — Marynowski et al. (2008); 10 — Marynowski et al. (2010), 11 — Racka et al., 2010 and the present paper: *.

was made by means of the Eltra standards. Calcium carbonate content was calculated as $CaCO_3 = 8.333 \times$ total inorganic carbon, assuming that all carbonates are present as calcite or aragonite.

Samples were Soxhlet-extracted with dichloromethane/methanol (DCM/Me) mixture (93:7 v:v) for 48 h in pre-extracted thimbles. Extracts were further separated using pre-washed thin layer chromatography (TLC) plates coated with silica gel (Merck, 20 × 20 × 0.25 cm). Prior to separation, the TLC plates were activated at 120 °C for 1 h. Plates were then loaded with the DCM soluble fraction and developed with *n*-hexane. The aliphatic hydrocarbon (R_f 0.4–1.0), aromatic hydrocarbon (R_f 0.05–0.4) and polar compound (R_f 0.0–0.05) fractions were collected for gas chromatography–mass spectrometry (GC–MS) analyses. The aliphatic and aromatic fractions of all samples were analyzed in further detail by gas chromatography–mass spectrometry. GC–MS analysis was performed on an Agilent 6890 gas chromatograph (EPC Cool On-Column Inlet) equipped with fused-silica capillary column (HP-5MS: 60 m × 0.32 mm × 0.25 μm). To improve separation of 2α-methylhopanes from hopanes we used semi-polar DB-17MS (60 m × 0.25 mm × 0.25 μm) capillary column. Helium was the carrier gas. Samples were injected on-column at 40 °C. The oven temperature was kept constant for 3 min, increased to 120 °C at 20 °C min^{-1}, subsequently to 300 °C at 3 °C min^{-1} and kept there for 35 min. The chromatograph was coupled to an Agilent 5973 Network with mass selective detector. The spectrometer was operated with an ion source temperature set at 200 °C, ionization energy of 70 eV and a cycle time of 1 s in the range *m/z* 50–700. The abundance of selected compounds was calculated by comparison of the peak area of an internal standard (9-phenylindene) with peak area of the individual hydrocarbons obtained from the GC–MS chromatograms using TIC mode. Peak identification was carried out by comparison of retention times with standards, mass spectra with the Wiley library, and spectra published elsewhere.

For confirmation of the GC–MS identification of 2α-methylhopanes we used GC–MS–MS method. This analysis was performed on an Agilent 7890A gas chromatograph coupled with an Agilent 7000 GC/MS Triple Quad instrument.

The GC was fitted with a HP1-MS column (60 m × 0.32 mm i.d., × 0.25 μm film thickness) and operated using He carrier gas at constant flow 2.6 mL/min. The inlet was held constant at 250 °C, while the GC oven was held at 40 °C for 1 min, then heated at 20 °C/min to 200 °C and at 1 °C min^{-1} to 280 °C, with an isothermal hold for 2 min. The MS ion source was at 230 °C and the quadrupole at 150 °C for all analyses. The ionization energy under electron impact was 70 eV.

3.6. Raman spectra collection

Raman measurements were performed using a confocal microscope alpha 300 R (WITec, GmbH, Ulm Germany) with a piezo scan stage (100 μm × 100 μm × 20 μm, PI, Germany). A frequency-doubled Nd:YAG laser (532 nm) was used for excitation. The system is equipped with a 100× microscope lens with numerical aperture = 0.90 (Nikon, Düsseldorf, Germany). The depth of focus was about 1 μm. Raman spectra were collected from the web-like structures on polished rock plates under 100× magnification. The measurements were performed by focusing the laser beam on the organic matter (OM) beneath the surface.

4. Results and discussion

4.1. Conodont biostratigraphy

The studied section from Kowala was subdivided biostratigraphically based on single occurrences of conodonts *Palmatolepis*, *Polygnathus* and *Icriodus* (Figs. 3 and A The on-line Supplementary Material section). The frequency of conodonts was low and could be a result of local conditions but could also be an effect of the widely-noted conodont crisis in the Early Famennian after the F/F event, when especially *Polygnathus* and *Palmatolepis* suffered major diversity and abundance decrease (Morrow, 2000). We established the age of this formation as Upper *triangularis*–Middle *crepida* zones within the early Famennian. The sample marked as KcIII/3 represented late *triangularis* zone reflecting the appearance of *Polygnathus volhynicus* (Dzik, 2006). This was the only sample, beside abundant KcIII/13, including *Palmatolepis*

Author's personal copy

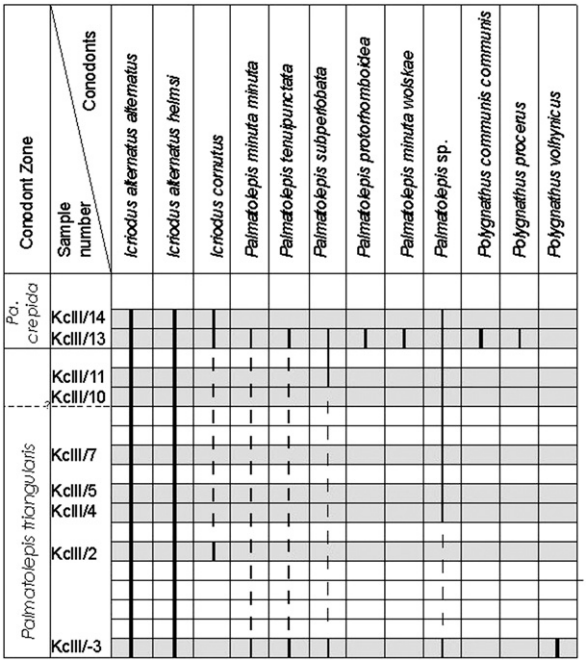

Fig. 3. Distribution of conodonts from the Lower Famennian of Kowala section.

minuta minuta species (see Fig. A The on-line Supplementary Material section) with the range of Upper *triangularis–trachytera* zone (Ziegler and Sandberg, 1990). It was obvious that the sample KcIII/13 represented zone *crepida* as indicated by *Palmatolepis minuta wolskae* with Middle–Upper *crepida* zone range (Ji and Ziegler, 1993) and by *Polygnathus communis communis* (Fig. A The on-line Supplementary Material section) which first appeared in the *crepida* zone (Matyja, 1993; Nehring-Lefeld et al., 2003). Overlying beds were not older than the *crepida* zone as defined by the appearance of *Polygnathus procerus* (Fig. A The on-line Supplementary Material section) with Upper *triangularis–crepida* zone range (Nehring-Lefeld, 1990; Matyja, 1993). An unequivocal establishment of the *triangularis*/*crepida* boundary was not possible because of a lack of indicator species. It was nearly certain that this boundary must exist between the KcIII/10 and KcIII/13 layers. As noted above, this second sample represented *crepida* zone, whereas KcIII/10 was problematic because of the presence of poorly-preserved species of *Palmatolepis*. However, this species revealed a similarity to *Palmatolepis wolskajae* with Middle–Upper *crepida* zone range (Ji and Ziegler, 1993), or perhaps was a transitional stage between *P. triangularis* and *P. wolskajae*. The boundary *triangularis*/*crepida* therefore might be placed between KcIII/7 and KcIII/10 layers. The biostratigraphic data based on conodonts corresponded with previous zonation based on acritarchs (Filipiak, 2009).

Filipiak (2009) described from this interval (samples KcIII/2, KcIII/7, KcIII/8, KcIII/14, and KcIII/18) *Puteoscortum willieriae* the index species for the Lower Famennian Pw acritarcha zone, which correspond to upper *triangularis–crepida* standard conodont zones and this is confirmed by the conodonts derived from the same samples (see Borcuch, 2006, and this paper). In addition Filipiak (2009) observed single occurrence of miospores *Cyrtospora cristifer* in sample KcIII/8, which is very important for palynostratigraphy supports this conclusions (see Filipiak, 2009; Fig. 4).

4.2. Microscopic observations

Examination of the petrographic thin-sections revealed that limestone samples did not exhibit stromatolitic-type laminations, however planar laminae did occur in some horizons (Fig. 4a). Detailed petrography showed that the organic matter was sporadically preserved; locally, organic remnants were at sufficient concentrations to suggest preservation akin to those ascribed to contemporary coccoid cyanobacterial mats (Fig. 4a and b). This OM habit was best resolved on limestone sections that are slightly polished and acid-etched with formic acid. Scanning electron microscope images of the sample surface revealed laminations which alternated between carbonaceous and more siliceous layers not atypical of microbial mat morphologies in modern samples. Characteristic features of the etched surfaces of the studied limestones included “pits” and “walls” that formed web-like structures especially resolvable within the silicate-rich layers (Fig. 4c–f). Irregular web-like patterns were readily recognizable on almost all etched surfaces of the sample (Fig. 4e–f). The walls usually ranged in thickness between 2 and 5 μm, and pits had various sizes (average diameter 10 to 15 μm); the smallest pit features were 3–10 μm and the largest was up to 35 μm in diameter. Energy-dispersive x-ray analyses demonstrated clear mineralogical differences between walls and pits consistent with the acid-etching process. The walls were composed primarily of calcium carbonate mixed with Al—Fe silicates and some Mg and K clays; in contrast, pits were composed of pure calcium carbonate. Web-like patterns are a common feature of modern coccoid cyanobacterial mats due to the progressive degradation of the cyanobacterial colony. Studies on decaying colonies of modern *Entophysalis* (Horodyski and Vonder Haar, 1975) and *Pleurocapsa* (Krumbein and Swart, 1983; Kempe and Kazmierczak, 1993) have shown that degradation of these colonial cyanobacteria is similarly selective and the resulting morphological forms reflect the more durable, thicker outer sheaths, which resemble such web-like structure. With regard to both morphology and mineral composition (e.g., clay content), web-like structures resembled those documented from early Silurian benthic cyanobacterial mats within black cherts (Kremer, 2006) as well as the Neoarchean carbonate rocks of South Africa (Kazmierczak et al., 2009). The OM observed was finely dispersed and difficult to detect using standard optical and scanning electron microscopy. However, OM can be clearly detected using Raman spectroscopy (e.g. Beyssac et al., 2003; Marshall et al., 2010). Raman spectra collected from the “webs” structures indicate the presence of carbonaceous matter within these structures (Fig. 4g).

4.3. Pyrite framboid diameter analysis

Studies of recent and ancient sediments revealed that the diameter distribution of pyrite framboids may be reliably used to indicate redox conditions (see Wilkin et al., 1996; Wignall and Newton, 1998; Racki et al., 2004; Wignall et al., 2005; Marynowski et al., 2007). A detailed description of the analytical procedure has been published by Wilkin et al. (1996) and Wignall and Newton (1998). Framboidal pyrite was common in all the samples we examined, with the exception of KcIII/2, KcIII/13, KcIII/19. In all samples, small-sized (<5 μm diameter) framboids that may have formed in a euxinic water column occurred, but larger (>5 μm diameter) framboids formed within the sediment below oxic or dysoxic water column were also present (see Fig. 5e, see also Fig. B in the online Supplementary Material section). Framboids exhibited a wide range of diameters, from 2.5 to 17.3 μm; mean value ranged from 5.1 to 7.0 μm (see Fig. 5e, see also Fig. B; Supplementary Material section). Samples from the lower part of the section (early Famennian; *triangularis* zone) were dominated by tiny framboids (<6 μm), and framboids>10 μm in diameter were rare. In contrast, within samples from the upper part of the sections (Lower *crepida* zone) small framboids were still numerous (e.g., in the samples KcIII/14 and KcIII/18 <6 μm were most common), however the majority of the framboids had larger diameters, and samples showed increased framboids >10 μm. Besides framboidal pyrite, other forms of pyrite (mainly euhedral crystals) occurred, albeit inconsistently. Although euhedral crystals occur in all samples, their frequency within samples was not constant. In samples from the lower part of the section their

Author's personal copy

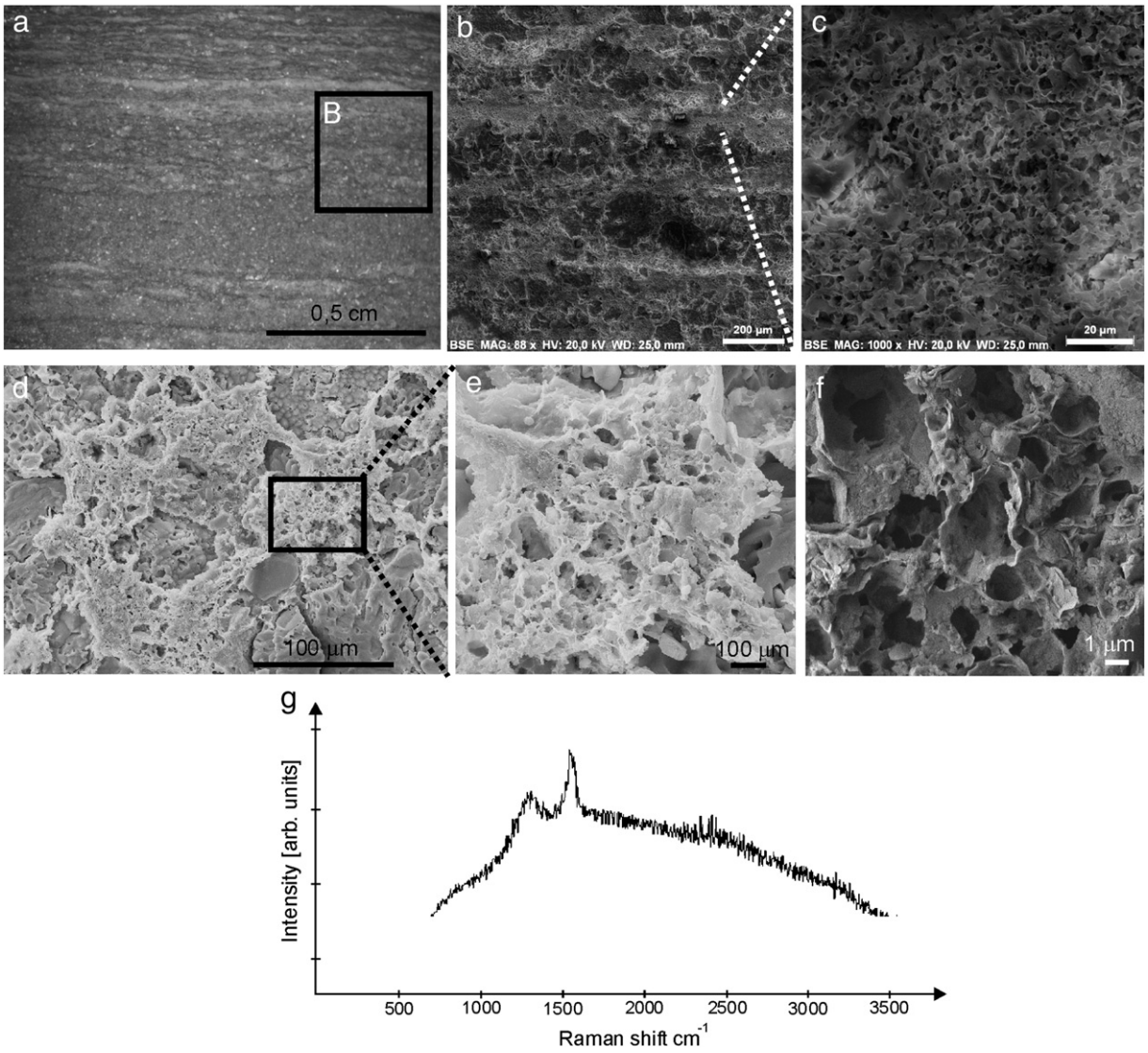

Fig. 4. Optical and SEM images of early Famenian limestones of Kowala. a — lamination of organic matter; photographed on the polished surface, b — enlarged fragment of a showing different composition of laminas, dark lamina — more carbonaceous and lighter lamina — more siliceous; c — fragment of siliceous lamina demonstrating web-like pattern; d — fragment of siliceous lamina with partly degraded fragments of cyanobacterial mat; e — magnified fragment of d showing web-like pattern representing mineralized mucus of cyanobacterial colony; and f — magnified other fragment of mineralized cyanobacterial mat. g — representative Raman spectrum of carbonaceous material obtained from web-like structure. a — reflected light in the stereoscopic microscope, b — and f — etched samples, SEM.

frequency is lower, while in the upper part of these sections the frequency increased.

4.4. General organic geochemical features

Bulk geochemical parameters, including total organic carbon and carbonate content, extractable OM concentration and parameters based on normal and branched alkanes are given in Table 1. The abundance of TOC for Early Famennian limestones and marly shales was in the range of 0.35 to 2.03%, but marly shales were generally enriched in organic carbon compared to limestones (Table 1; Fig. 5a). Data for vitrinite reflectance R_r (%), temperature of maximum release of hydrocarbons (T_{max}) and hydrogen (HI) and oxygen (OI) indexes have been presented elsewhere for neighboring portions of the Kowala section (Marynowski et al., 2001, 2007; Marynowski and Filipiak, 2007). Samples were generally immature, to low-mature with T_{max} values ranging from 416 to 439 °C (Joachimski et al., 2001; Marynowski et al., 2007, 2010; Marynowski and Filipiak, 2007) and an average vitrinite reflectance value of 0.53% R_r (Marynowski et al., 2001). The immaturity to low-maturity of the OM was confirmed using measures of mono- and triaromatic steroids (MA and TA; Table 1). Moderate values of TA/(MA + TA), ranging from 0.5 to 0.6 and very low values of TA(I)/TA(I + II), not exceeding 0.04, are typical for thermally non-altered sedimentary rocks (Peters et al., 2005).

In the Kowala Quarry there was no any evidence of hydrocarbon migration through the investigated sections based on low to moderate extractable amounts (Table 1) and low values of production index (Joachimski et al., 2001; Marynowski et al., 2007; Marynowski and Filipiak, 2007), as well as the low OM maturity mentioned above (Marynowski, 1999; Racka et al., 2010). All these lines of evidence confirm the syngeneity of the extractable organic matter. Hydrogen Index data and the HI vs. T_{max} plot (Marynowski et al., 2007; Marynowski and Filipiak, 2007) indicated a mixture of type I–II kerogens. The average extractable OM composition was similar to that reported previously (Marynowski et al., 2007; Marynowski and Filipiak, 2007; Marynowski et al., 2008, 2010) and consisted of ~20–30% aliphatic hydrocarbons, ~15–30% aromatic hydrocarbons, and ~45–50% polar compounds (Table 1). The preponderance of polar compounds was typical for immature to low-mature OM (Tissot and Welte, 1984). *N*-alkane carbon preference index (CPI) values were

Author's personal copy

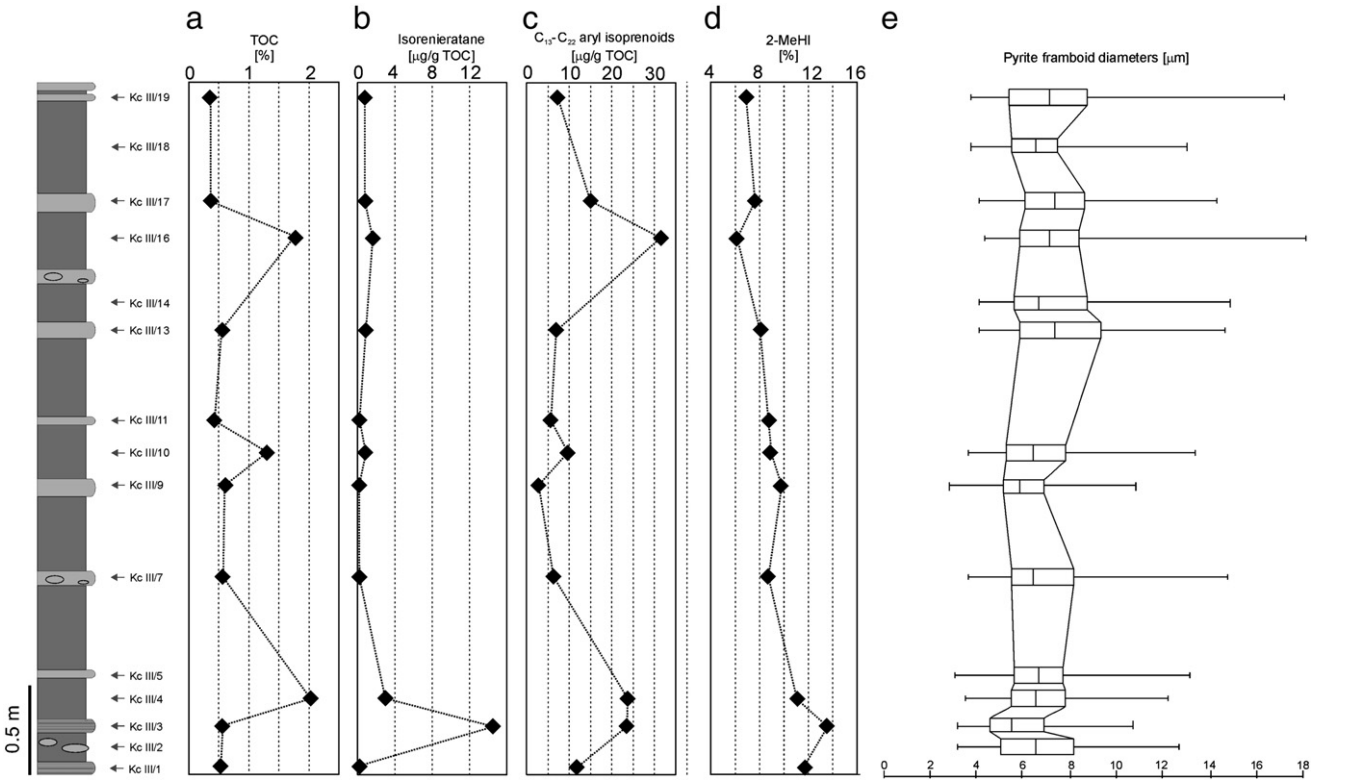

Fig. 5. Composite plot of the Early Famennian Kowala section showing organic carbon, biomarkers and pyrite analyses data. (a) Total organic carbon content — TOC (%). (b) Isorenieratane concentration (μg/g TOC). (c) C_{13}–C_{22} aryl isoprenoids concentration (μg/g TOC). (d) 2MeHI = 2α-methylhopane/(C_{30} 17α(H)-hopane + 2α-methylhopane) ratio (in percents). (e) Box-and-whisker plots of the pyrite framboid size diameters.

approximately 1, with the exception of samples KcIII/1, KcIII/7, KcIII/9 and KcIII/11 for which $CPI_{(25–31)}$ value ranged from 1.16 to 1.23, suggesting insignificant terrestrial input. Moreover, other biomarkers characteristic for terrestrial OM were not detected in the investigated samples, which is in agreement with data presented by Filipiak (2009). This study revealed a very high dominance of marine-derived prasinophytes and acritarchs (>80%) over land-derived miospores. In the rest of the sample pattern with high-molecular-weight, odd-carbon number preponderance *n*-alkanes, characteristics for land-derived OM were not detected. In contrast, during the Middle Famennian sedimentation of the limestones and marly shales with pyritized fauna (Marynowski et al., 2007) and Upper Famennian Hangenberg event (Marynowski and Filipiak, 2007), the $CPI_{(25–31)}$ values for many samples were higher than 1.20, reaching even 1.7, which clearly indicated terrestrial OM input.

The distribution of the isoprenoids (pristane and phytane) relative to *n*-alkanes, was similar to Middle Famennian limestones and marly shales (Marynowski et al., 2007) and organic-rich samples from the Upper Famennian profile (Marynowski and Filipiak, 2007). As a rule, samples exhibited Pr/*n*-C_{17}>2.0 and Ph/*n*-C_{18} ratios>1.5 (Table 1). In all the samples, the abundance of Pr and Ph was greater than the abundance of *n*-alkanes (Fig. C The on-line Supplementary Material

Table 1
Bulk geochemical data, percentage yields of fractions and basic molecular parameters.

Sample	TOC (%)	CC (%)	EOM (mg/g TOC)	Fractions			$CPI_{(Total)}$	$CPI_{(25–31)}$	Pr/Ph	Pr/nC_{17}	Ph/nC_{18}	SCh/LCh	TA/(MA + TA)	TA(I)/TA(I + II)
				AL (%)	AR (%)	POL (%)								
KcIII/1	0.52	84.13	93	38	17	45	1.11	1.16	2.4	4.3	2.0	2.1	0.56	0.03
KcIII/3	0.55	88.58	96	30	23	47	1.08	1.04	1.7	4.4	3.1	2.2	0.63	0.03
KcIII/4	2.03	59.61	75	23	32	45	1.12	1.09	2.4	4.7	2.4	2.5	0.53	0.04
KcIII/7	0.55	88.65	79	25	23	52	1.11	1.22	1.8	4.1	2.2	2.0	0.55	0.04
KcIII/9	0.61	84.75	80	27	14	59	1.10	1.23	2.5	3.8	1.6	2.5	0.64	0.03
KcIII/10	1.30	51.45	91	25	20	55	1.10	1.12	2.8	3.9	1.6	2.9	0.50	0.04
KcIII/11	0.46	87.04	81	20	20	60	1.09	1.18	2.3	4.2	1.9	2.2	0.61	0.04
KcIII/13	0.56	89.29	56	48	18	34	1.07	1.10	2.3	4.6	2.1	2.3	0.59	0.03
KcIII/16	1.78	57.07	59	26	27	46	1.12	1.11	2.5	4.1	2.2	2.3	0.50	0.04
KcIII/17	0.37	90.00	64	25	20	55	1.05	1.08	2.0	3.3	1.9	3.1	0.54	0.03
KcIII/19	0.35	85.53	72	27	22	51	1.08	1.10	2.1	3.5	1.9	3.0	0.55	0.03

TOC — total organic carbon.
CC — carbonate content.
EOM — extractable organic matter.
Al — aliphatic, Ar — aromatic and POL — polar.
CPI — carbon preference index, Pr — pristane and Ph — phitane.
SCh/LCh — short chain to long chain *n*-alkanes ratio: ($nC_{17} + nC_{18} + nC_{19}$)/($nC_{27} + nC_{28} + nC_{29}$).
TA/(MA + TA) — triaromatic steroids (TA) to sum of triaromatic — (TA) and monoaromatic steroids (MA) ratio (Peters et al., 2005).
TA(I)/TA(I + II) — short chain triaromatic steroids TA(I) to short- and long-chain triaromatic steroids ratio (Peters et al., 2005).

Author's personal copy

section). Moreover, similar to what was shown previously (Brown and Kenig, 2004; Marynowski and Filipiak, 2007, and discussion therein), the Pr/Ph ratios in the investigated samples did not indicate changes in the redox conditions during sedimentation (Didyk et al., 1978), but rather changes in the source of the OM (Brown and Kenig, 2004, and discussion therein). For example, most recent studies show that pristane, the major isoprenoid in all Kowala samples, probably formed from α-tocopherol in quite anoxic sedimentary conditions (Rontani et al., 2010). The ratio of short chain to long chain *n*-alkanes (SCh/LCh) >2 indicated a preponderance of the low molecular weight *n*-alkanes (Fig. C The on-line Supplementary Material section), which in the immature, to low-mature samples has been documented to be a general characteristic for marine OM (e.g. Peters et al., 2005).

4.5. Stable isotopic composition

The $\delta^{13}C_{carb}$ and $\delta^{13}C_{TOC}$ values were quite uniform for all analyzed samples and were in agreement with those presented by Joachimski et al. (2001) forming a consistent continuation of their F/F section. For example, $\delta^{13}C_{carb}$ values in Upper *triangularis* zone were between 0 to 0.5‰; $\delta^{13}C_{TOC}$ ranged between −30 and −29‰ (Joachimski et al., 2001); our study revealed values from 0 to 1‰ and from −30 to −29‰, respectively (Fig. 6b). Moreover, similar $\delta^{13}C_{carb}$ values were recorded by Joachimski in Lower Famennian at Płucki section (see Racki et al., 2002). On the other hand, the $\delta^{13}C_{carb}$ values we observed were c.a. 1‰ lower than those from the other Central and Southern Europe locations (Buggisch and Joachimski, 2006).

4.6. Molecular composition

Samples contained a high abundance of sterane and hopane biomarkes (Fig. 7a; Table 1); the ratio of all steranes to all hopanes approached 1, as is characteristic for shelf basin facies of the Devonian sedimentary rocks from the Holy Cross Mountains (Marynowski et al., 2000). Distribution of hopanes was similar to that previously described (Marynowski et al., 2000, 2007; Marynowski and Filipiak, 2007) with dominant C_{30}-17α,21β-hopane and a gradual decrease in the abundance of homohopane epimers ($C_{31}S+R$ homologues dominated) with increased carbon number (Fig. 7a). All samples contained minor amounts of gammacerane (Fig. 7a), as indicated by the gammacerane/C_{30}-17α-hopane ratio (Table 2). With respect to regular steranes, compounds with C_{27} to C_{31} carbon atoms were present, with C_{29} steranes dominating. However, although C_{29} sterane homologues predominated over C_{27} and C_{28} steranes their origin is not necessarily connected with terrestrial organic material, as sometimes interpreted (Jiao et al., 2009; see Huang and Meinschein, 1979). Sterols with 29 carbon atoms, precursors of C_{29} steranes, have been reported from photosynthetic algae cell membranes (e.g. Volkman et al., 1998) and the distribution of steranes with C_{29} homologues is well known from many typically marine sedimentary rocks (e.g. Peters et al., 2005; Volkman, 2005; Wang et al., 2008). Moreover, we did not find other terrestrial biomarkers in the samples outside of high molecular weight *n*-alkanes with an odd carbon number dominating in only few samples. Other steroid biomarkers were represented by: C_{28}–C_{30} methylsteranes with a base peak at *m/z* 231, C_{29}–C_{31} steranes with a base peak at *m/z* 245 and C_{30}–C_{32} steranes with a base peak at *m/z* 259 (Dahl et al., 1992, 1995; Chen and Summons, 2001; see also Marynowski and Filipiak, 2007). As observed with the desmethyl steranes, all series were dominated by 5α,14α,17α(H)-20R isomers. Aromatic biomarkers were represented by mono- and triaromatic steroids (Peters et al., 2005), including triaromatic analogs of C_{21}–C_{26} 20-*n*-alkylpregnanes.

4.6.1. Cyanobacteria biomarkers

All samples contained abundant homologous series of 2α-methylhopanes (Summons and Jahnke, 1990), extending from C_{28} through C_{34} and dominated by C_{30} to C_{32} homologues (Fig. 7a and c). Such compounds are commonly considered as biomarkers of cyanobacterial activity (Summons et al., 1999), and their precursors were also recently detected in some anoxygenic phototrophs (Rashby et al., 2007; see also discussion in Wakeham et al., 2007). The 2α-methylhopane index (Summons et al., 1999; Table 2) ranged from 6.1 to 13.4% and generally decreased upward through the section. Other typical methanotroph methylhopanes such as 3β-methylhopanes

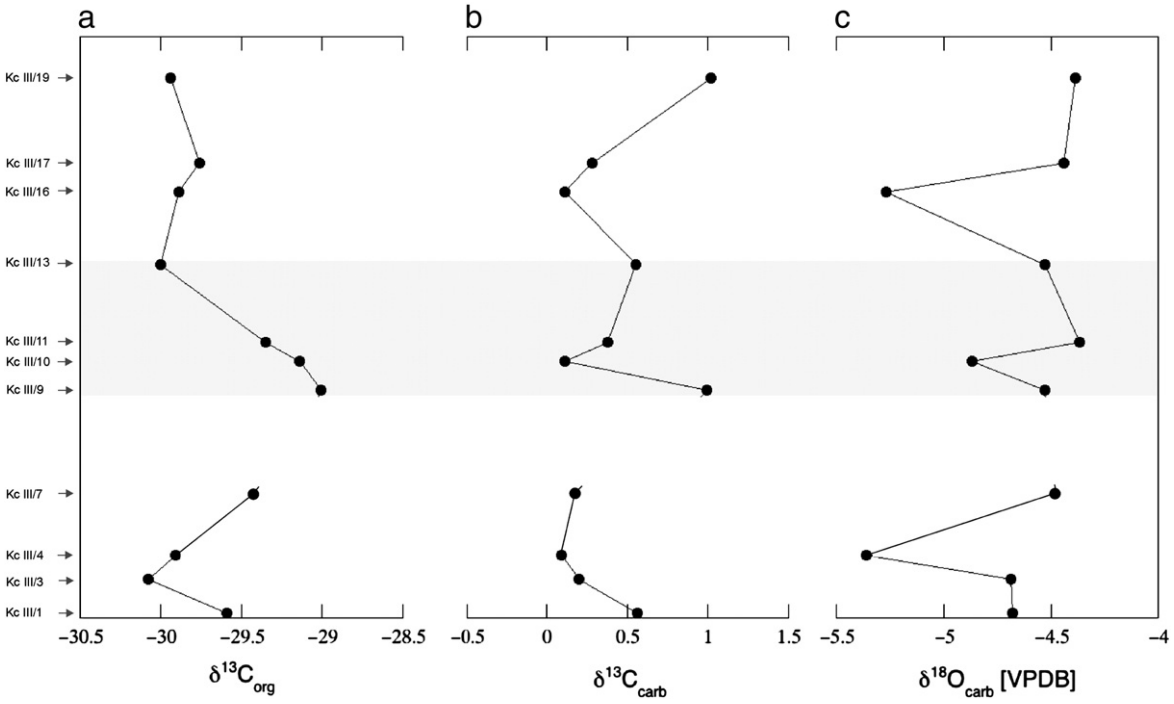

Fig. 6. Variations in carbon isotopic composition of: (a) total organic carbon and (b) bulk carbonates and variations in oxygen isotopic composition of: (c) bulk carbonates. Shaded area reflected shifts towards low values seen at the beginning of the period of diminished photic zone anoxia.

Author's personal copy

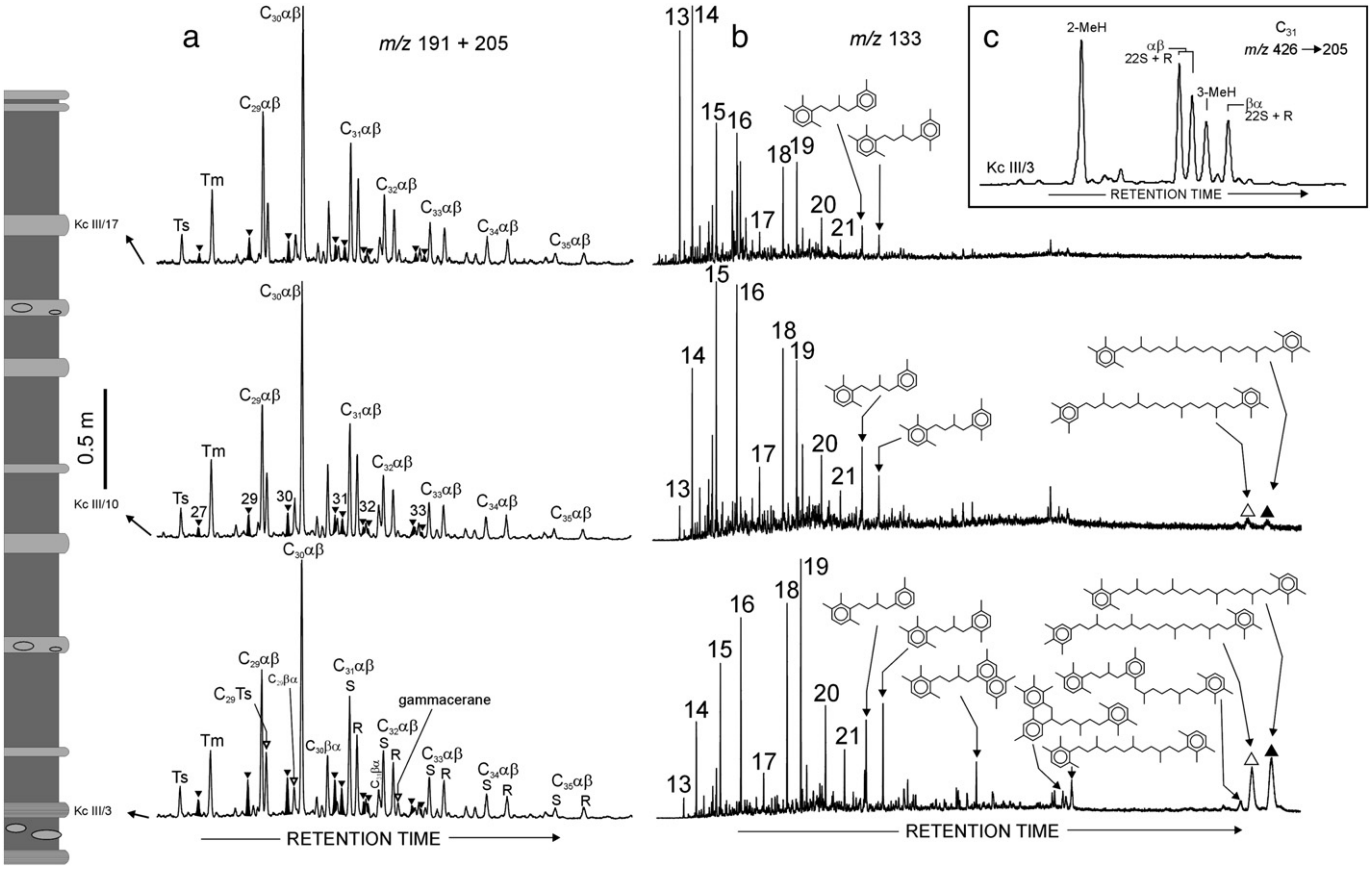

Fig. 7. Partial mass chromatograms of (b) *m/z* 133 showing the distribution of isorenieratane (filled triangle), 2,3,6-/3,4,5-TM substituted diaryl isoprenoid (open triangle) and their related derivatives including aryl isoprenoids (numbers identify individual carbon number pseudohomologs) in the three samples from the Early Famennian Kowala section. Note the gradual decrease of isorenieratane and 2,3,6-/3,4,5-TM substituted diaryl isoprenoid upward the section. HP-5MS column was used. (a) Partial mass chromatograms of the *m/z* 191 + 205 showing hopanes and methylhopanes distributions in the investigated samples. Note the gradual decrease of 2α-methylhopanes upward the section. Filled peaks and black triangles denote 2α-methylhopanes with the carbon number not including the additional methyl group. Ts = 18α(H)-22,29,30-trisnorneohopane, Tm = 17α(H)-22,29,30-trisnorhopane. DB-17 column was used. (c) Methylhopane distribution from the KcIII/3 sample using the GC–MS–MS method. Compound abbreviations: 2-MeH = 2α-methyl-17α(H)-hopane, 3-MeH = 2β-methyl-17α(H)-hopane. The 22S and 22R epimers are shown for C_{31}-homohopanes. An HP-1 column was used.

(e.g. Farrimond et al., 2004) were detected in much lower levels (Fig. 7c). In addition, samples contained monomethyl alkanes (MMAs) ranging from C_{15} to C_{21} (Fig. C The on-line Supplementary Material section) in distributions similar to those described by Bauersachs et al. (2009). MMA series contained from 2-, to 7-MMAs with dominant 6- + 7-MMAs isomers (Fig. C The on-line Supplementary Material section). The mid-chain branched MMAs are compounds characteristic for modern and ancient cyanobacteria (e.g. Kenig et al., 1995; Köster et al., 1999; Bauersachs et al., 2009; Scherf and Rullkötter, 2009).

Table 2
Aryl isoprenoids, isorenieratane, concentrations and molecular parameters based on *n*-alkanes, hopanes, methylhopanes, steranes and aryl isoprenoid distributions.

Sample	Isoren. (μg/g TOC)	Isoren. + 2,3,6-/3,4,5-DAI (μg/g TOC)	C_{13}–C_{22} aryl isoprenoids (μg/g TOC)	Gammacerane/ C_{30} 17α-hopane ratio	AIR	∑hop/∑alk	Ster/17α-hop.	2MHPI	2MHP/ster
KcIII/1	0.0	0.0	11.75	0.02	1.41	0.16	0.75	11.8	0.04
KcIII/3	14.5	24.3	23.53	0.05	0.69	0.11	0.95	13.4	0.04
KcIII/4	3.1	6.0	23.74	0.04	2.14	0.10	1.00	11.0	0.03
KcIII/7	0.0	0.0	6.15	0.02	0.90	0.11	0.90	8.4	0.03
KcIII/9	0.0	0.0	2.78	0.04	0.49	0.14	0.91	9.7	0.03
KcIII/10	0.8	1.9	9.66	0.03	1.36	0.14	0.97	8.9	0.02
KcIII/11	0.0	0.0	5.36	0.05	1.24	0.16	0.89	8.6	0.02
KcIII/13	0.9	1.9	6.97	0.04	0.73	0.14	0.87	8.0	0.02
KcIII/16	1.6	3.3	31.56	0.03	4.48	0.11	1.07	6.1	0.01
KcIII/17	0.8	1.6	15.02	0.04	2.56	0.12	0.85	7.7	0.02
KcIII/19	0.9	1.5	6.94	0.04	0.60	0.13	0.96	6.9	0.01

Isoren. — Isorenieratane.
2.3.6-/3.4.5-DAI — 2.3.6-/3.4.5-diaryl isoprenoid.
AIR — Aryl isoprenoid ratio: $(C_{13}–C_{17})/(C_{18}–C_{22})$ (Schwark and Frimmel, 2004).
Ster/17α-hop — regular steranes consist of the C_{27}·C_{28}·C_{29} ααα(20 S + 20R) and αββ(20 S + 20R).
17α-hopanes consist of the C_{29} to C_{33} pseudohomolog (including 22S and 22R epimers).
∑hop/∑alk — hopanes/*n*-alkanes ratio.
2MHPI — 2α-methylhopane/(2α-methylhopane + αβ-hopane) × 100 (Summons et al., 1999).
2MHP/ster — 2α-methylhopane/all steranes ratio (Xie et al., 2005).

Author's personal copy

4.6.2. Green sulfur bacteria biomarkers

Sedimentary rocks from the analyzed section contained diverse concentrations of the green sulfur bacteria biomarker — isorenieratane (Fig. 7b), in amounts ranging from ~0 to 14.5 μg/g TOC. This compound, together with 2.3.6-/3.4.5-diaryl isoprenoid (an additional possible GSB biomarker; Requejo et al., 1992; Clifford et al., 1998) is characteristic for Upper Devonian shelf basin sequences (Marynowski et al., 2000; Joachimski et al., 2001; Brown and Kenig, 2004; Hartkopf-Fröder et al., 2007), and was detected in the other Kowala sections (Joachimski et al., 2001; Marynowski et al., 2007; Marynowski and Filipiak, 2007; Marynowski et al., 2008, 2010). Moreover, the data in Table 2 show that differences in the isorenieratane concentration are consistent with differences in the sum of isorenieratane plus 2,3,6-/3,4,5-TM substituted diaryl isoprenoids. In addition, samples contained diagenetic products of both diaryl isoprenoids, including dominated aryl isoprenoids (Fig. 7b), in concentrations ranging from 6.9 to 31.6 μg/g TOC (Table 2). The values of the aryl isoprenoid ratio (Schwark and Frimmel, 2004, see Table 2), were small for limestones and relatively high for marly shales, the one exception being sample KcIII/17 (Table 2).

5. Implications

5.1. Water column structure: A biomarker and pyrite framboid approach

Values of Th/U ratio, an indicator of benthic water oxygenation (Wignall and Myers, 1988) published by Bond and Zatoń (2003) and Bond et al. (2004) ranged between 1 and 4 for the Upper *triangularis* zone and increased gradually, reaching 3 to 5 for the *crepida* zone. We interpret these data to reflect a change from suboxic to oxic bottom water through the *triangularis* and *crepida* zones. In addition, geochemical proxies published by Racki et al. (2002) suggested dysoxic bottom water conditions during the Middle *triangularis* conodont zone with low productivity and no volcanic or hydrothermal input.

Our biomarker data, which included the presence of isorenieratane and 2,3,6-/3,4,5-TM substituted diaryl isoprenoid in almost all samples (Fig. 5, Table 2), supported by the occurrence of aryl isoprenoids (Table 2) suggested the occurrence of water column euxinia during the deposition of sediments corresponding to the *triangularis* and *crepida* zones. Isorenieratane is known as an early diagenetic product of isorenieratene — diaryl carotenoid and is biosynthesized by the brown strain of green sulfur bacteria (GSB) (Liaaen-Jensen, 1978). These bacteria are obligately anaerobic and require both light and H_2S (Summons and Powell, 1987; Hartgers et al., 1994; Koopmans et al., 1996; see Sinninghe Damsté and Schouten, 2005 in review). The other characteristic biomarker which confirmed the hypothesis of stratified water column present in our samples is gammacerane (Table 2; Fig. 7a), a compound derived from bacterivorous ciliates grazing on bacteria, including GSB (Sinninghe Damsté et al., 1995; see also Peters et al., 2005; Marynowski and Filipiak, 2007; Sepúlveda et al., 2009; Racka et al., 2010).

Pyrite framboids revealed that small-sized (<6 μm diameter) framboids were present in all investigated samples. Such tiny framboids were formed in the anoxic portion of the water column (Muramoto et al., 1991, see also Wignall and Newton, 1998). In the lower part of the Early Famennian section (samples KcIII/2 and KcIII/3), <6 μm diameter framboids dominate, though larger framboids are present (Fig. B; Supplementary data). However in the *crepida* zone >6 μm diameter framboids dominated with increasing examples of >10 μm indicate increasing seafloor ventilation. These data suggest that in the lower part of the section the prevalence of small framboids indicated water column euxinia, but the co-occurrence of larger framboids in the same populations revealed sediments with overlying oxygenated waters (see Algeo et al., 2011 for comparison). In the upper part of the section small framboids occurred but the percentage of larger diameters increased, suggesting a stepwise oxygenation of bottom waters.

In summary, euxinic conditions occurred in the upper part of the water column during the deposition of the Early Famennian sediments, as confirmed by the presence of green sulfur bacteria biomarkers (Figs. 5 and 7; Table 2) and the occurrence of tiny framboids. The bottom waters of the time were oxygenated, at least briefly, as indicated by Th/U ratio (Bond and Zatoń, 2003; Bond et al., 2004), geochemical proxies (Racki et al., 2002), as well as the presence of large framboids (Fig. B; online Supplementary Material section) and implied cyanobacterial mats and low numbers of benthic fauna. We propose the schematic reconstruction shown in Fig. 8; in this model, both the lower and upper portions of the section imply water column anoxia. In contrast to the lower portion (Upper *triangularis* zone) within which suboxic bottom water and upper water persistent anoxia, in the upper part (Lower *crepida* zone) anoxia was intermittent and bottom waters were much relatively well oxygenated.

The presence of benthic cyanobacterial mats at the bottom of Early Famennian shelf basin indicated oxic or dysoxic conditions in the zone above the sediment. Depending on the intensity of photosynthesis, the rate of oxygen production could have varied from high to very low making possible dysoxic (microaerophilic) conditions at the cyanobacterial mat surface. However, we cannot exclude temporally anoxic conditions near the bottom (Kremer and Kaźmierczak, 2005; Welander et al., 2010) and even short episodes of GSB growing on the seafloor (Fig. 8), but based on pyrite framboids data, Th/U ratio and paleontological observations we suggest that bottom water conditions were mainly suboxic even to oxic which eliminated GSB as seafloor bacterial community. A gradual increase of bottom water oxygenation, together with presence of biomarkers of cyanobacteria and bentic fauna increases support of the above scenario. Considering the presence of photosynthetic cyanobacteria benthic mats, the waters of the Early Famennian shelf basin must have been relatively shallow, and the photic zone must have reached the sediment–water interface. Early Famennian Upper *triangularis*/Lower *crepida* zones represent a transgression (Johnson et al., 1986) and emphasize a relatively shallow depth basinal sedimentation.

The shift from a suboxic to oxic bottom waters may be reflected in the carbon stable isotope values of the organic carbon and carbonate within the measured strata (Fig. 6). Suboxic bottom waters impede respiration and lead to the accumulation of OM partially in the form of thickened cyanobacterial mats. When respiration rates are low, the $\delta^{13}C$ value of the dissolved CO_2 available for photosynthesis will be affected and will reflect the limited supply of compounds for respiration. However, when respiration rates are high, the $\delta^{13}C$ value of the dissolved CO_2 available to photosynthesizers may change, due to the wide variety of substrates subject to active respiration. For these reasons, we might expect a change in the isotopic composition of photosynthesizers with a change from suboxic to oxic bottom waters. This is complicated by the wide range of other sources and sinks in the marine organic and inorganic carbon pool. The shift towards low $\delta^{13}C$ values seen at the beginning of the period of diminished photic zone (shaded area within Fig. 6), might reflect an influx of newly respired CO_2 to surface waters, caused by enhanced respiration at depth.

However, the shift from a suboxic to oxic bottom waters did not influence the phytoplankton assemblage which is uniform, abundant and diverse within the investigated section and unchanging between the Upper *triangularis* and Lower *crepida* zones (see Filipiak, 2009). In contrast to the late Middle Ordovician Platteville and Decorah Formations (Pancost et al., 1998), in which the ratio of 2α-methylhopane to hopane showed a negative correlation with aryl isoprenoid relative abundance, our samples revealed no correlation (Fig. 5). This may suggest that cyanobacterial mats grew near the bottom where oxic to suboxic and maybe also episodically anoxic

Author's personal copy

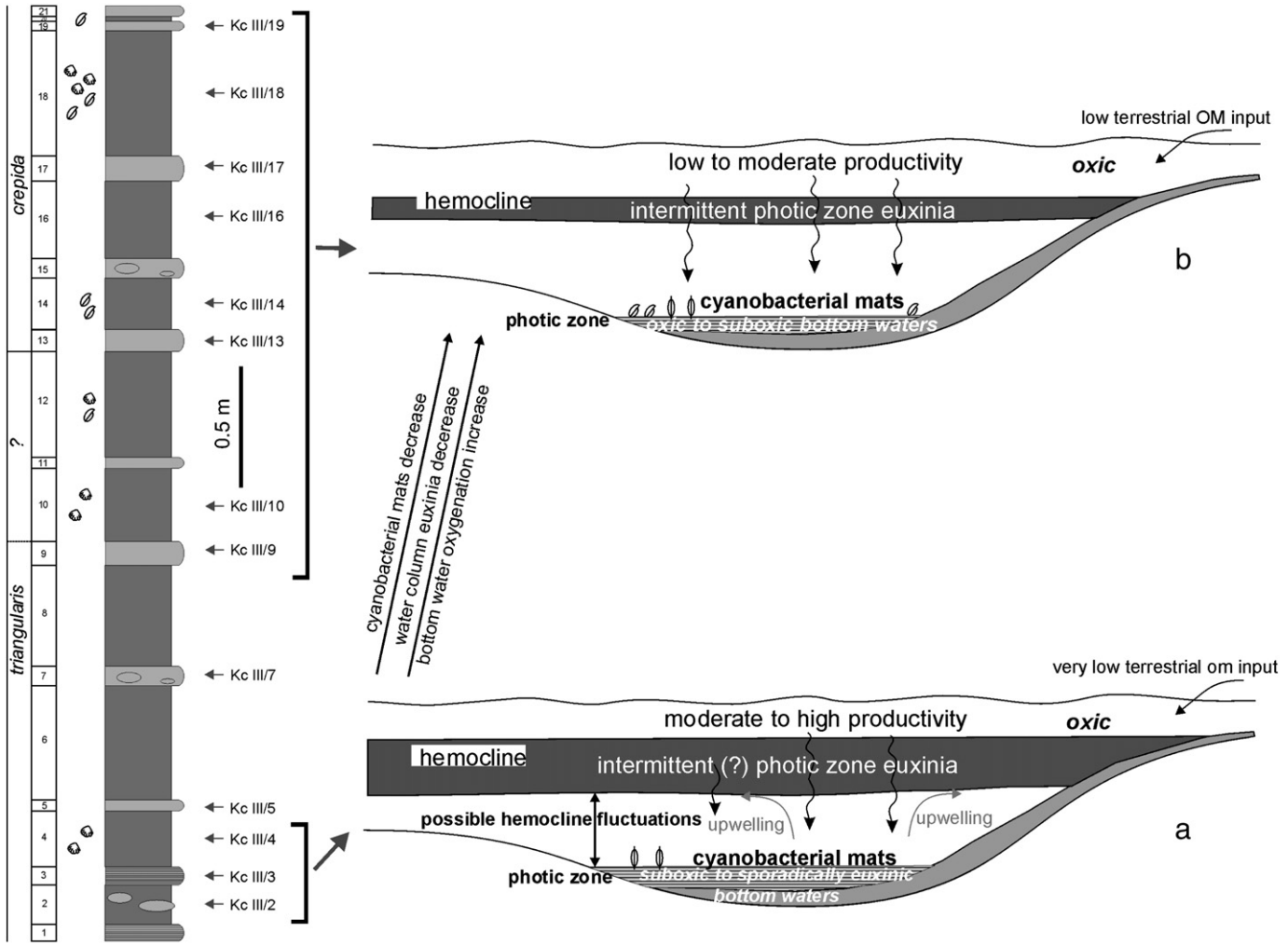

Fig. 8. Schematic diagram of a depositional model to clarify changes in the Early Famennian succession in the Holy Cross Mountains shelf basin. For section legend see Fig. 1.

conditions prevailed while GSB lived within the anoxic portion of the water column (Fig. 8). The similar model, with intermittently euxinic conditions in the intermediate water mass (oxygen minimum zone) and suboxic to weakly anoxic conditions at the seafloor was most recently proposed for the Late Permian to Early Triassic Ubara section from Japan (Algeo et al., 2011).

5.2. Cyanobacteria after the F/F mass extinction

Cyanobacterial mats are especially present in the marine environment in coastal environments (Stal, 2001) and proliferate under a specific set of environmental conditions. For this reason, increased microbial activity during the Phanerozoic has frequently been posited to occur after episodes of faunal mass extinction. Biomarker study on such global extinction intervals has reinforced this hypothesis (Xie et al., 2005; Wang, 2007; Jiao et al., 2009). Other studies have shown the presence of post-extinction microbial build-up in the Early Triassic (e.g. Schubert and Bottjer, 1992; Pruss and Bottjer, 2004; Hips and Haas, 2006; Mary and Woods, 2008), as well as microbial carbonates in the Frasnian/Famennian mass extinction horizon (Whalen et al., 2002) and during the Famennian (Becker et al., 1991; Wood, 2000; Stephens and Sumner, 2003; Shen and Webb, 2004).

The data presented here comprise yet another confirmation that microbial activity increased significantly after a global mass extinction event. We believe that cyanobacteria grew in the Early Famennian shelf basin (Figs. 5 and 8) after the F/F boundary (in *triangularis* zone) and gradually decreased in activity during the subsequent *crepida* zone (Fig. 5). Joachimski et al. (2001) did not quantify cyanobacterial biomarkers in their investigations of the F/F section, while Playford et al. (1984), Becker et al. (1991), Chen and Tucker (2003) and other authors reported common occurrences of microbial cyanobacterial structures in the sediments of the same age. This implies that an understanding of the role of cyanobacteria after the F/F mass extinction still requires future interdisciplinary study, particularly on cyanobacteria occurrence and growth changes in time. Rashby et al. (2007) and Wakeham et al. (2007) have shown that some anoxygenic phototrophic bacteria may produce hopanoids methylated at C-2. However, we have revealed the presence of other biomarkers such as the monomethyl alkanes characteristic for cyanobacteria and the independent microscopic data showing the web-like structures (Fig. 4), which confirms the presence of cyanobacteria in the Lower Famennian of the Holy Cross Mountains.

6. Conclusions

The geochemical and petrographical study of the basinal Lower Famennian Kowala section showed a change from anoxic–suboxic to oxic bottom water through *triangularis* and *crepida* zones. Occurrence of morphological web-like structures typical for microbial mats and presence of cyanobacteria biomarkers such as 2α-methylhopanes and monomethyl alkanes implied microbial activity after the global F/F extinction event. Moreover, the implied presence of cyanobacterial

Author's personal copy

mats suggests the prevalence of suboxic to oxic but photic bottom water conditions, as confirmed by large pyrite framboids and high values of Th/U ratio. Simultaneously, common occurrence of green sulfur bacteria biomarkers such as isorenieratane and derivatives thereof, in addition to the presence of small pyrite framboids suggested that portions of the water column were at least intermittently euxinic.

Supplementary materials related to this article can be found online at doi:10.1016/j.palaeo.2011.03.018.

Acknowledgements

Ms. Ewa Teper (Faculty of Earth Sciences, Sosnowiec) is acknowledged for her help during analyses using ESEM. Thanks are also expressed to R. Stark (TU Darmstadt) for the Raman analyses. This work has been financed by MNISW grants: NN307 4272 34 (to MR) and NN307 2379 33 (to LM). MR wishes to acknowledge the European Social Fund (UPGOW scholarship) for financial support. The Department of Earth and Environmental Sciences and the GeoBio-Center of LMU Munich are greatly acknowledged for offering working facilities. A. v. Humboldt Foundation is appreciated for support to BK.

References

Algeo, T.J., Kuwahara, K., Sano, H., Bates, S., Lyons, T., Elswick, E., Hinnov, L., Ellwood, B., Moser, J., Maynard, J.B., 2011. Spatial variation in sediment fluxes, redox conditions, and productivity in the Permian–Triassic Panthalassic Ocean. Palaeogeography, Palaeoclimatology, Palaeoecology. doi:10.1016/j.palaeo.2010.07.007.

Baud, A., Richoz, S., Marcoux, J., 2005. Calcimicrobial cap rocks from the basal Triassic units: western Taurus occurrences (SW Turkey). Comptes Rendus Palevol 4, 569–582.

Baud, A., Richoz, S., Pruss, S., 2007. The lower Triassic anachronistic carbonate facies in space and time. Global and Planetary Change 55, 81–89.

Bauersachs, T., Kremer, B., Schouten, S., Sinninghe Damsté, J.S., 2009. A biomarker and $\delta^{15}N$ study of thermally altered Silurian cyanobacterial mats. Organic Geochemistry 40, 149–157.

Becker, R.T., House, M.R., Kirchgasser, W.T., Playford, P.E., 1991. Sedimentary and faunal changes across the Frasnian/Famennian boundary in the Canning Basin of Western Australia. Historical Biology 5, 183–196.

Berkowski, B., 2002. Famennian Rugosa and Heterocorallia from Southern Poland. Palaeontologia Polonica 61, 3–88.

Beyssac, O., Goffe, B., Petitet, J.-P., Froigneux, E., Moreau, M., Rouzaud, J.-N., 2003. On the characterization of disordered and heterogeneous carbonaceous materials by Raman spectroscopy. Spectrochimica Acta Part A 59, 2267–2276.

Bond, D., 2006. The fate of the homoctenids (Tentaculitoidea) during the Frasnian–Famennian mass extinction (Late Devonian). Geobiology 4, 167–177.

Bond, D., Zatoń, M., 2003. Gamma-ray spectrometry across the Upper Devonian basin succession at Kowala in the Holy Cross Mountains (Poland). Acta Geologica Polonica 53, 93–99.

Bond, D., Wignall, P.B., Racki, G., 2004. Extent and duration of marine anoxia during the Frasnian–Famennian (Late Devonian) mass extinction in Poland, Germany, Austria and France. Geological Magazine 141, 173–193.

Borcuch, E., 2006. Górnodewońskie konodonty z Gór Świętokrzyskich — aspekt paleoekologii i biostratygrafii na przykładzie profili Kostomłotów i Kowali. MSc thesis, Silesian University, in Polish, 1–39.

Boutton, T.W., 1991. Stable carbon isotope ratios of natural materials: I. Sample preparation and mass spectrometric analysis. In: Coleman, D.C., Fry, B. (Eds.), Carbon Isotope Techniques. Academic Press, New York, pp. 155–171.

Brown, T.C., Kenig, F., 2004. Water column structure during deposition of Middle Devonian–Lower Mississippian black and green/grey shales of the Illinois and Michigan Basin: a biomarker approach. Palaeogeography, Palaeoclimatology, Palaeoecology 215, 59–85.

Buggisch, W., Joachimski, M.M., 2006. Carbon isotope stratigraphy of the Devonian of Central and Southern Europe. Palaeogeography, Palaeoclimatology, Palaeoecology 240, 68–88.

Chen, J., Summons, R., 2001. Complex patterns if steroidal biomarkers in Tertiary lacustrine sediments of the Biyang Basin, China. Organic Geochemistry 32, 115–126.

Chen, D., Tucker, M.E., 2003. The Frasnian–Famennian mass extinction: insights from high-resolution sequence stratigraphy and cyclostratigraphy in South China. Palaeogeography, Palaeoclimatology, Palaeoecology 193, 87–111.

Clifford, D.J., Clayton, J.L., Sinninghe Damsté, J.S., 1998. 2,3,6-/3,4,5-Trimethyl substituted diaryl carotenoid derivatives (Chlorobiaceae) in petroleums of the Belarussian Pripyat River Basin. Organic Geochemistry 29, 1253–1267.

Dahl, J., Moldowan, M.J., Mccaffrey, M.A., Lipton, P., 1992. A new class of natural products revealed by 3β-alkyl steranes in petroleum. Nature 355, 154–157.

Dahl, J., Moldowan, M.J., Summons, R., Mccaffrey, M.A., Lipton, P., Watt, D.S., Hope, J.M., 1995. Extended 3β-alkyl steranes and 3-alkyl triaromatic steroids in crude oils and rock extracts. Geochimica et Cosmochimica Acta 59, 3717–3729.

Didyk, B.M., Simoneit, B.R.T., Brassell, S.C., Eglinton, G., 1978. Organic geochemical indicators of palaeoenvironmental conditions of sedimentation. Nature 272, 216–222.

Dzik, J., 2002. Emergence and collapse of the Frasnian conodont and ammonoid communities in the Holy Cross Mountains, Poland. Acta Palaeontologica Polonica 47, 565–650.

Dzik, J., 2006. The Famennian "Golden Age" of conodonts and ammonoids in the Polish part of the Variscan sea. Palaeontologia Polonica 63, 1–359.

Farrimond, P., Talbot, H.M., Watson, D.F., Schulz, L.K., Wilhelms, A., 2004. Methylhopanoids: molecular indicators of ancient bacteria and a petroleum correlation tool. Geochimica et Cosmochimica Acta 68, 3873–3882.

Filipiak, P., 2002. Palynofacies around the Frasnian/Famennian boundary in the Holy Cross Mountains, southern Poland. Palaeogeography, Palaeoclimatology, Palaeoecology 181, 313–324.

Filipiak, P., 2009. Lower Famennian phytoplankton from the Holy Cross Mountains, Central Poland. Review of Palaeobotany and Palynology 157, 326–338.

Ginter, M., 2002. Chondrichthyan fauna of the Frasnian–Famennian boundary beds in Poland. Acta Palaeontologica Polonica 47, 329–338.

Girard, C., Lécuyer, Ch., 2002. Variations in Ce anomalies of conodonts through the Frasnian/Famennian boundary of Poland (Kowala — Holy Cross Mountains): implications for the redox state of seawater and biodiversity. Palaeogeography, Palaeoclimatology, Palaeoecology 181, 299–311.

Halamski, A.T., Baliński, A., 2009. Latest Famennian brachiopods from Kowala, Holy Cross Mountains, Poland. Acta Palaeontologica Polonica 54, 289–306.

Hartgers, W.A., Sinninghe Damsté, J.S., Requejo, A.G., Allan, J., Hayes, J.M., Yue, Ling, Xie, T.-M., Primack, J., de Leeuw, J.W., 1994. A molecular and carbon isotopic study towards the origin and diagenetic fate of diaromatic carotenoids. Organic Geochemistry 22, 703–725.

Hartkopf-Fröder, C., Kloppisch, M., Mann, U., Neumann-Mahlkau, P., Schaefer, R.G., Wilkes, H., 2007. The end-Frasnian mass extinction in the Eifel Mountains, Germany: new insights from organic matter composition and preservation. In: Becker, R.T., Kirchgasser, W.T. (Eds.), Devonian events and correlations: Geological Society, London, Special Publications, 278, pp. 173–196.

Hips, K., Haas, J., 2006. Calcimicrobial stromatolites at the Permian–Triassic boundary in a western Tethyan section, Bükk Mountains, Hungary. Sedimentary Geology 185, 239–253.

Horodyski, R.J., Vonder Haar, S., 1975. Recent calcareous stromatolites from Laguna Mormona, Baja California. Journal of Sedimentary Research 45, 894–906.

House, M.R., 2002. Strength, timing, setting and cause of mid-Palaeozoic extinctions. Palaeogeography, Palaeoclimatology, Palaeoecology 181, 5–25.

Huang, W.-Y., Meinschein, W.G., 1979. Sterols as ecological indicators. Geochimica et Cosmochimica Acta 43, 739–745.

Ji, Q., Ziegler, W., 1993. Lali section: an excellent reference section for Upper Devonian in south China. Courier Forschungs-Institut Senckenberg 157, 1–183.

Jiao, D., Perry, R.S., Engel, M.H., Sephton, M.A., 2009. Biomarker indicators of bacterial activity and organic fluxes during end Triassic mass extinction event. Proceedings of SPIE — the International Society for. Optical Engineering 7097. doi:10.1117/12.796160.

Joachimski, M.M., Ostertag-Henning, C., Pancost, R.D., Strauss, H., Freeman, K.H., Littke, R., Sinninghe Damsté, J.S., Racki, G., 2001. Water column anoxia, enhanced productivity and concomitant changes in δ13C and δ34S across the Frasnian–Famennian boundary (Kowala — Holy Cross Mountains/Poland). Chemical Geology 175, 109–131.

Joachimski, M.M., Pancost, R.D., Freeman, K.H., Ostertag-Henning, C., Buggisch, W., 2002. Carbon isotope geochemistry of the Frasnian–Famennian transition. Palaeogeography, Palaeoclimatology, Palaeoecology 181, 91–109.

Johnson, J.G., Klapper, G., Sandberg, C.A., 1986. Late Devonian eustatic cycles around margin of Old Red Continent. Annales de la Societe geologique de Belgique 109, 141–147.

Kazmierczak, J., Altermann, W., Kremer, B., Kempe, S., Eriksson, P.G., 2009. Mass occurrence of benthic coccoid cyanobacteria and their role in the production of Neoarchean carbonates of South Africa. Precambrian Research 173, 79–92.

Kempe, S., Kazmierczak, J., 1993. Satonda Crater Lake, Indonesia: hydrogeochemistry and biocarbonates. Facies 28, 1–32.

Kenig, F., Sinninghe Damsté, J.S., Kock-van Dalen, A.C., Rijpstra, W.I.C., Huc, A.Y., de Leeuw, J.W., 1995. Occurrence and origin of mono-, di-, and trimethylalkanes in modern and Holocene cyanobacterial mats from Abu Dhabi, United Arab Emirates. Geochimica et Cosmochimica Acta 59, 2999–3015.

Kershaw, S., Zhang, T., Lan, G., 1999. A ?microbialite carbonate crust at the Permian–Triassic boundary in South China, and its palaeoenvironmental significance. Palaeogeography, Palaeoclimatology, Palaeoecology 146, 1–18.

Kershaw, S., Li, Y., Crasquin-Soleau, S., Feng, Q., Mu, X., Collin, P.-Y., Reynolds, A., Guo, L., 2007. Earliest Triassic microbialites in the South China block and other areas: controls on their growth and distribution. Facies 53, 409–425.

Koopmans, M.P., Köster, J., van Kaam-Peters, H.M.E., Kenig, F., Schouten, S., Hartgers, W.A., de Leeuw, J.W., Sinninghe Damsté, J.S., 1996. Diagenetic and catagenetic products of isorenieratene: molecular indicators for photic zone anoxia. Geochimica et Cosmochimica Acta 60, 4467–4496.

Köster, J., Volkman, J.K., Rullkötter, J., Scholz-Böttcher, B.M., Rethmeier, J., Fischer, U., 1999. Mono-, di- and trimethyl-branched alkanes in cultures of the filamentous cyanobacterium *Calothrix scopulorum*. Organic Geochemistry 30, 1367–1379.

Kremer, B., 2006. Mat-forming coccoid cyanobacteria from early Silurian marine deposits of Sudetes, Poland. Acta Palaeontologica Polonica 51, 143–154.

Author's personal copy

Kremer, B., Kaźmierczak, J., 2005. Cyanobacterial mats from Silurian black Radiolarian cherts: phototrophic life at the edge of darkness? Journal of Sedimentary Research 75, 895–904.

Krumbein, W.E., Swart, P.K., 1983. The microbial carbon cycle. In: Krumbein, W.E. (Ed.), Microbial Geochemistry. Blackwell Sci. Publ., Oxford, pp. 5–62.

Lehrmann, D.J., Payne, J.L., Felix, S.V., Dillett, P.M., Wang, H., Yu, Y., Wei, J., 2003. Permian–Triassic boundary sections from shallow-marine carbonate platforms of the Nanpanjiang Basin, South China: implications for oceanic conditions associated with the End-Permian extinction and its aftermath. Palaios 18, 138–152.

Liaaen-Jensen, S., 1978. Chemistry of karotenoid pigments. In: Clayton, R.K., Sistrom, W.R. (Eds.), Photosynthetic Bacteria. Plenum Press, New York, pp. 233–247.

Marshall, C.P., Edwards, H.G.M., Jehlicka, J., 2010. Understanding the application of Raman spectroscopy to the detection of traces of life. Astrobiology 10, 229–243.

Mary, M., Woods, A.D., 2008. Stromatolites of the Lower Triassic Union Wash Formation, CA: evidence for continued post-extinction environmental stress in western North America through the Spathian. Palaeogeography, Palaeoclimatology, Palaeoecology 261, 78–86.

Marynowski, L., 1999. Stopień przeobrażenia termicznego materii organicznej w skałach dewonu Gór Świętokrzyskich. Przegląd Geologiczny 47, 1125–1129.

Marynowski, L., Filipiak, P., 2007. Water column euxinia and wildfire evidence during deposition of the Upper Famennian Hangenberg event horizon from the Holy Cross Mountains (central Poland). Geological Magazine 144, 569–595.

Marynowski, L., Narkiewicz, M., Grelowski, C., 2000. Biomarkers as environmental indicators in a carbonate complex, examples from the Middle Devonian, the Holy Cross Mountains, Poland. Sedimentary Geology 137, 187–212.

Marynowski, L., Czechowski, F., Simoneit, B.R.T., 2001. Phenylnaphthalenes and polyphenyls in Palaeozoic source rocks of the Holy Cross Mountains, Poland. Organic Geochemistry 32, 69–85.

Marynowski, L., Rakociński, M., Zatoń, M., 2007. Middle Famennian (Late Devonian) interval with pyritized fauna from the Holy Cross Mountains (Poland): organic geochemistry and pyrite framboid diameter study. Geochemical Journal 41, 187–200.

Marynowski, L., Filipiak, P., Pisarzowska, A., 2008. Organic geochemistry and palynofacies of the Early–Middle Frasnian transition (Late Devonian) of the Holy Cross Mts, southern Poland. Palaeogeography, Palaeoclimatology, Palaeoecology 269, 152–165.

Marynowski, L., Filipiak, P., Zatoń, M., 2010. Geochemical and palynological study of the Upper Famennian Dasberg event horizon from the Holy Cross Mountains (central Poland). Geological Magazine 147, 527–550.

Matyja, H., 1993. Upper Devonian of western Pomerania. Acta Geologica Polonica 43, 27–94.

McCrea, J.M., 1950. On the isotopic chemistry of carbonates and a paleotemperature scale. Journal of Chemical Physics 18, 849–857.

Morrow, J., 2000. Shelf-to-basin lithofacies and conodont paleoecology across Frasnian–Famennian (F/F, mid-Late Devonian) boundary, central Great Basin (western USA). Courier Forschungs-Institut Senckenberg 219, 1–57.

Muramoto, J.A., Honjo, S., Fry, B., Hay, B.J., Howarth, R.W., Cisne, J.L., 1991. Sulfur, iron and organic carbon fluxes in the Black Sea — sulfur isotopic evidence for origin of sulfur fluxes. Deep-Sea Research Part A—Oceanographic Research Papers 38, S1151–S1187.

Narkiewicz, M., 1988. Turning points in sedimentary development in the Late Devonian in southern Poland. In: McMillan, N.J., Embry, A.F., Glass, D.J. (Eds.), Devonian of the world: Proceedings of the International Symposium on the Devonian System, 14, pp. 619–635. Calgary.

Nehring-Lefeld, H., 1990. Biostratygrafia famenu z otworu wiertniczego Kowala 1 na podstawie konodontów. Kwartalnik Geologiczny 34, 271–290.

Nehring-Lefeld, H., Malec, J., Woroncowa-Marcinowska, T., Matyja, H., Haydukiewicz, J., Chorowska, M., 2003. Conodonta. In: Sarnecka, E. (Ed.), Budowa Geologiczna Polski, III, 1b, pp. 536–606.

Pancost, R.D., Freeman, K.H., Patzkowsky, M.E., Wavrek, D.A., Collister, J.W., 1998. Molecular indicators of redox and marine photoautotroph composition in the late Middle Ordovician of Iowa, U.S.A. Organic Geochemistry 29, 1649–1662.

Peters, K.E., Walters, C.C., Moldowan, J.M., 2005. The Biomarker Guide, Vol. 2. Cambridge University Press, p. 1155.

Playford, P.E., McLaren, D.J., Orth, C.J., Gilmore, J.S., Goodfellow, W.D., 1984. Iridium anomaly in the Upper Devonian of the Canning basin, Western Australia. Science 226, 437–439.

Pruss, S.B., Bottjer, D.J., 2004. Late Early Triassic microbial reefs of the western United States: a description and model for their deposition in the aftermath of the end-Permian mass extinction. Palaeogeography, Palaeoclimatology, Palaeoecology 211, 127–137.

Racka, M., Marynowski, L., Filipiak, P., Sobstel, M., Pisarzowska, A., Bond, D.P.J., 2010. Double anoxia in the Late Famennian (Devonian) of the Holy Cross Mountains (Poland): the Annulata events. Palaeogeography, Palaeoclimatology, Palaeoecology 297, 549–575.

Racki, G., Baliński, A., 1998. Late Frasnian Atrypida (Brachiopoda) from Poland and the Frasnian–Famennian biotic crisis. Acta Palaeontologica Polonica 43, 273–304.

Racki, G., Szulczewski, M., 1996. Stop 4. Kowala Railroad Cut and Quarry. Sixth European Conodont Symposium (ECOS VI), Excursion Guide. In: Szulczewski, M., Skompski, S. (Eds.), Instytut Paleobiologii PAN, Warszawa, pp. 27–33.

Racki, G., Racka, M., Matyja, H., Devleeschouwer, X., 2002. The Frasnian/Famennian boundary interval in the South Polish–Moravian shelf basins; integrated event-stratigraphical approach. Palaeogeography, Palaeoclimatology, Palaeoecology 181, 251–297.

Racki, G., Piechota, A., Bond, D., Wignall, P.B., 2004. Geochemical and ecological aspects of lower Frasnian pyrite-goniatite level at Kostomłoty (Holy Cross Mountains, Central Poland). Geological Quarterly 48, 267–282.

Rashby, S.E., Sessions, A.L., Summons, R.E., Newman, D.K., 2007. Biosynthesis of 2-methylbacteriohopanepolyols by an anoxygenic phototroph. PNAS 104, 15099–15104.

Requejo, A.G., Allan, J., Creany, S., Gray, N.R., Cole, K.S., 1992. Aryl isoprenoids and diaromatic carotenoids in Paleozoic source rocks and oils from the Western Canada and Williston basins. Organic Geochemistry 23, 205–222.

Rontani, J.-F., Nassiry, M., Michotey, V., Guasco, S., Bonin, P., 2010. Formation of pristane from α-tocopherol under simulated anoxic sedimentary conditions: a combination of biotic and abiotic degradative processes. Geochimica et Cosmochimica Acta 74, 252–263.

Sartenaer, P., Racki, G., Szulczewski, M., 1998. The late Frasnian rhynchonellid genus *Pammegetherhynchus* (Brachiopoda) in Poland, and its relevance to the Kellwasser Crisis. Acta Palaeontologica Polonica 43, 379–394.

Scherf, A.-K., Rullkötter, J., 2009. Biogeochemistry of high salinity microbial mats — part 1: lipid composition of microbial mats across intertidal flats of Abu Dhabi, United Arab Emirates. Organic Geochemistry 40, 1018–1028.

Schubert, J.K., Bottjer, D.J., 1992. Early Triassic stromatolites as post-mass extinction disaster forms. Geology 20, 883–886.

Schwark, L., Frimmel, A., 2004. Chemostratigraphy of the Posidonia Black Shale, SW-Germany II. Assessment of extent and persistence of photic-zone anoxia using aryl isoprenoid distribution. Chemical Geology 206, 231–248.

Sepúlveda, J., Wendler, J., Leider, A., Kuss, H.-J., Summons, R.E., Hinrichs, K.-U., 2009. Molecular isotopic evidence of environmental and ecological changes across the Cenomanian–Turonian boundary in the Levant Platform of central Jordan. Organic Geochemistry 40, 553–568.

Sharp, Z., 2006. Principles of Stable Isotope Geochemistry: Upper Saddle River. New Jersey, Prentice Hall. 360 pp.

Sheehan, P.M., Harris, M.T., 2004. Microbialite resurgence after the Late Ordovician extinction. Nature 430, 75–78.

Shen, J.-W., Webb, G.E., 2004. Famennian (Upper Devonian) stromatolite reefs at Shatang, Guilin, Guangxi, South China. Sedimentary Geology 170, 63–84.

Sinninghe Damsté, J.S., Schouten, S., 2005. Biological markers for anoxia in the photic zone of the water column. The Handbook of Environmental Chemistry 2, 1–37.

Sinninghe Damsté, J.S., Kenig, F., Koopmans, M.P., Köster, J., Schouten, S., Hayes, J.M., de Leeuw, J.W., 1995. Evidence for gammacerane as an indicator of water column stratification. Geochimica et Cosmochimica Acta 59, 1895–1900.

Stal, L.J., 2001. Coastal microbial mats: the physiology of a small-scale ecosystem. South African Journal of Botany 67, 399–410.

Stephens, N.P., Sumner, D.Y., 2003. Famennian microbial reef facies, Napier and Oscar Ranges, Canning Basin, western Australia. Sedimentology 50, 1283–1302.

Summons, R.E., Jahnke, L.L., 1990. Identification of the methylhopanes in sediments and petroleum. Geochimica et Cosmochimica Acta 54, 247–251.

Summons, R.E., Powell, T.G., 1987. Identification of aryl isoprenoids in source rocks and crude oils: biological markers for the green sulfur bacteria. Geochimica et Cosmochimica Acta 51, 557–566.

Summons, R.E., Jahnke, L.L., Hope, J.M., Logan, G.A., 1999. 2-Methylhopanoids as biomarkers for cyanobacterial oxygenic photosynthesis. Nature 400, 554–557.

Szulczewski, M., 1971. Upper Devonian conodonts, stratigraphy and facial development in the Holy Cross Mts. Acta Geologica Polonica 21, 1–129.

Szulczewski, M., 1995. Depositional evolution of the Holy Cross Mts. (Poland) in the Devonian and Carboniferous — a review. Geological Quarterly 39, 471–488.

Tissot, B.P., Welte, D.H., 1984. Petroleum Formation and Occurrence2nd edn. Springer Verlag, Berlin. 669 pp.

Vishnevskaya, V., Pisera, A., Racki, G., 2002. Siliceous biota (radiolarians and sponges) and the Late Devonian biotic crisis: the Polish reference. Acta Palaeontologica Polonica 47, 211–226.

Volkman, J.K., 2005. Sterols and other triterpenoids: source specificity and evolution of biosynthetic pathways. Organic Geochemistry 36, 139–159.

Volkman, J.K., Barrett, S.M., Blackburn, S.I., Mansour, M.P., Sikes, E.L., Gelin, F., 1998. Microalgal biomarkers: a review of recent research developments. Organic Geochemistry 29, 1163–1179.

Wakeham, S.G., Amann, R., Freeman, K.H., Hopmans, E.C., Jørgensen, B.B., Putnam, I.F., Schouten, S., Sinninghe Damsté, J.S., Talbot, H.A., Woebken, D., 2007. Microbial ecology of the stratified water column of the Black Sea as revealed by a comprehensive biomarker study. Organic Geochemistry 38, 2070–2097.

Wang, Ch., 2007. Anomalous hopane distributions at the Permian–Triassic boundary, Meishan, China — evidence for the end-Permian marine ecosystem collapse. Organic Geochemistry 38, 52–66.

Wang, T.-G., He, F., Wang, Ch., Zhang, W., Wang, J., 2008. Oil filling history of the Ordovician oil reservoir in the major part of the Tahe Oilfield, Tarim Basin, NW China. Organic Geochemistry 39, 1637–1646.

Welander, P.V., Coleman, M.L., Sessions, A.L., Summons, R.E., Newman, D.K., 2010. Identification of a methylase required for 2-methylhopanoid production and implications for the interpretation of sedimentary hopanes. PNAS 107, 8537–8542.

Whalen, M.T., Day, J., Eberli, G.P., Homewood, P.W., 2002. Microbial carbonates as indicators of environmental change and biotic crises in carbonate systems: examples from the Late Devonian, Alberta Basin, Canada. Palaeogeography, Palaeoclimatology, Palaeoecology 181, 127–151.

Wignall, P.B., Myers, K.J., 1988. Interpreting bentic oxygen levels in mudrocks — a new approach. Geology 16, 452–455.

Wignall, P.B., Newton, R., 1998. Pyrite framboid diameter as a measure of oxygen-deficiency in ancient mudrocks. American Journal of Science 298, 537–552.

Wignall, P.B., Newton, R., Brookfield, M.E., 2005. Pyrite framboid evidence for oxygen-poor deposition during the Permian–Triassic crisis in Kashmir. Palaeogeography, Palaeoclimatology, Palaeoecology 216, 183–188.

Author's personal copy

Wilkin, R.T., Barnes, H.L., Brantley, S.L., 1996. The size distribution of framboidal pyrite in modern sediments: an indicator of redox conditions. Geochimica et Cosmochimica Acta 60, 3897–3912.
Wood, R., 2000. Novel paleoecology of a postextinction reef: Famennian (Late Devonian) of the Canning Basin, northwestern Australia. Geology 28, 987–990.
Woods, A.D., Baud, A., 2008. Anachronistic facies froma drowned Lower Triassic carbonate platform: lower member of the Alwa Formation (Ba'id Exotic), Oman Mountains. Sedimentary Geology 209, 1–14.
Xie, S., Pancost, R.D., Yin, H., Wang, H., Evarshed, R.P., 2005. Two episodes of microbial change coupled with Permo/Triassic faunal mass extinction. Nature 434, 494–497.
Xie, S., Pancost, R.D., Huang, J.H., Wignall, P.B., Yu, J., Tang, X., Chen, L., Huang, X., Lai, X., 2007. Changes in the global carbon cycle occurred as two episodes during the Permian–Triassic crisis. Geology 35, 1083–1086.
Xie, S., Pancost, R.D., Yin, H., Wang, H., Yang, H., Wignall, P.B., Luo, G., Jia, C., Chen, L., 2010. Cyanobacterial blooms tied to volcanism during the 5 m.y. Permo-Triassic biotic crisis. Geology 38, 447–450.
Ziegler, W., Sandberg, C.A., 1990. The Late Devonian standard conodont zonation. Courier Forschungs-Institut Senckenberg 121, 1–115.